SIZE CONTROLLED SYNTHESIS OF SnO_2 NANOPARTICLES: FACILE SOLVOTHERMAL PROCESS

K. ANANDAN*, V. RAJENDRAN
Department of physics, Presidency College, Chennai-600 005, Tamil Nadu, India

Tetragonal phase SnO_2 nanocrystals were synthesized via facile solvothermal process by using $SnCl_4.5H_2O$ and HCl at different temperature. The phase, size and purity of the resultant products were characterized by means of powder X-ray diffraction (XRD). Optical studies were carried by UV-Vis absorption and photoluminescence (PL). The morphology was confirmed by scanning electron microscopy (SEM) analysis. Transmission electron microscopy (TEM) and High-resolution transmission electron microscopy (HR-TEM) were discussed for as-synthesized samples. The decreasing preparation temperatures on nanoparticle upon the decreasing particle size are well presented for the as-synthesized samples. The growth mechanisms and special properties relative to the SnO_2 nanostructured are discussed. Our results suggest that the temperature plays an important role to growth nanoparticles.

(Received April 5, 2010; accepted May 5, 2010)

Keywords: Semiconductors, Tin oxide, Nanomaterials, Temperature effect, Facile solvothermal;

1. Introduction

SnO_2 is an important n-type wide-energy-gap semiconductor (Eg = 3.64 eV) which has a wide range of application such as solid-state gas sensors [1], transparent conducting electrodes [2], rechargeable Li batteries [3] and optical electronic devices [4]. During the past decade, SnO_2 nanostructures have been one of the most important oxide nanostructures due to their properties and potential application [5].

Many methods have been developed for the synthesis of SnO_2 nanoparticles [6-8]. Among various methods, solvothermal is well suited for production of nanostructure materials, because of its relatively low processing cost, much milder and the ability to control the grain size. In this paper, we have synthesized of SnO_2 nanoparticles and described the effect of temperature in solvothermal method. The starting materials are very cheap and the synthesis procedures are simple, and the obtained SnO_2 particles are in nanometer scale and small size of nanoparticles. This should be a better choice instead of the sol–gel method from tin alkoxides. The particles have been characterized by means of XRD, UV-Vis, PL, SEM, TEM and HR-TEM.

2. Experimental

The experimental was followed by a facile solvothermal process. All chemicals are analytical grade and are used as received without further purification. In a typical procedure, after dissolving 0.81g of tin chloride (hydrous $SnCl_4.5H_2O$) in 2ml of concentrated hydrochloric acid in a autoclave with capacity of 50ml. Then 15ml of absolute ethanol was added into the autoclave. The autoclave was sealed and maintained at 120°C for 15h, then cooled to room temperature naturally. A greenish yellow precipitate was collected and washed with deionized water and absolute ethanol several times to remove impurity. The final product was dried in vacuum at 60°C

for 5h sample (a). For comparison, sample (b) and (c) were also synthesized in the same way except that 200°C and 250°C maintained instead of 120°C.

The crystalline phase and size of the products were determined by X–ray powder diffraction (XRD) by using a Seifert (JSO-DEBYEFLEX 2002) diffractometer with Cu-Kα radiation (λ=0.1540nm). A scan rate of 0.04º /s was applied to record the pattern in the 2θ range of 20 - 70º. Optical absorbance of the sample was recorded by a UV-Vis Varian Cary 5E spectrophotometer. Photoluminescence (PL) measurements were carried out on a Fluoromax-4 spectrofluorometer with a Xe lamp as the excitation light source. Scanning electron microscopy (SEM) performed on a Hitachi S-4500 scanning electron microscope, was used to observe the morphology of the as-synthesized samples. High-resolution transmission electron microscope (HRTEM) and transmission electron microscope (TEM) was taken with a JEOL-3010 operating at 200KV.

3. Results and discussion

Fig. 1 shows the XRD patterns of the as-prepared samples at different temperatures (120, 200 and 250°C, respectively). All diffraction peaks can be readily indexed to tetragonal SnO_2 nanoparticles. No other peaks were observed such as Sn or any other Sn based oxide, which indicating the high purity of the samples. The diffraction peaks are markedly broadened, which indicates that the crystalline sizes of samples are very small. According to the Debye-Scherer's equation

$$D_{hkl} = \frac{0.89\lambda}{(\beta\cos\theta)}$$

where the λ is X-ray wavelength (0.1540nm for Cu-Kα), β is the width at half maximum of the diffraction peak (fwhm) and θ is Bragg diffraction angle. The crystallite sizes were calculated to be 2.4, 4.5 and 4.9nm for the samples prepared at temperature 120, 200 and 250°C respectively. The crystallite sizes were reveals that clearly with decreasing preparation temperature, the crystallite size gradually decreases.

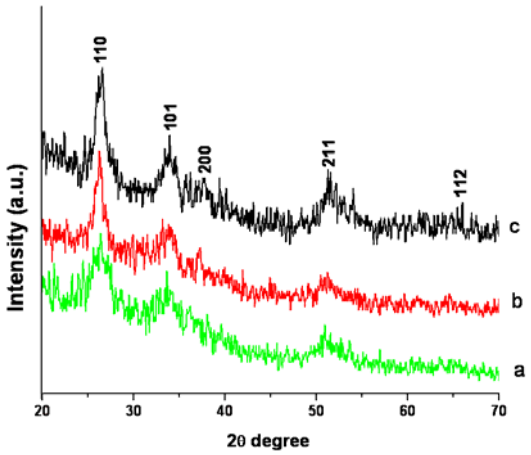

Fig. 1. XRD pattern of SnO_2 nanoparticles prepared at different temperatures, (a) 120°C, (b) 200°C and (c) 250°C.

Fig. 2 shows the optical absorbance spectra of the as-synthesized samples (a), (b) and (c). The size of SnO_2 nanocrystallites is smaller or comparable to the exciton Bohr radius (2.7nm), the quantum confinement effect would occur and blue shift in energy is observed, for the sample (a) well obtained the quantum confinement effect. The band gap energy is found to be particle size dependent and increases with decreasing particle size. The value of the absorption edge of the

samples (a), (b) and (c) was 260, 278 and 285nm blue shift were observed respectively, the band gap energy for the samples can be obtained by extrapolation of the rising part to the plot to the x-axis. The corresponding band gap energy to be calculated 4.76, 4.46 and 4.35eV, which larger than the value of 3.6eV for the bulk SnO_2 [4]. The increasing trends of the band gap energy upon the decreasing particles size are well presented for the as-synthesized samples.

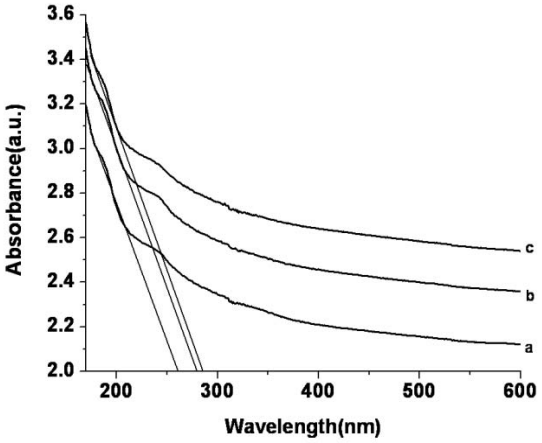

Fig. 2. UV-Vis absorption spectra of the SnO_2 nanoparticles at different temperatures.

Generally, in poly- and nano-crystalline oxides, oxygen vacancies are known to be the most common defects and usually act as radiative centers in luminescence processes. The oxygen vacancies present in three different charge states: V_o^0, V_o^+ and V_o^{2+} [9] in the oxide. As V_o^0 is a very shallow donor, the most oxygen vacancies will be in their paramagnetic V_o^+ state under flat-band conditions. The peaks might also come from the luminescence center of tin interstitials or dangling etc. in the present SnO_2 nanoparticles [10]. The earlier reports supposed that the broad peaks around 400-500nm can be assumed to be due to the formation of a V_o^{++} luminescent center in the SnO_2 nanocrystal and nanorod [5]. In this paper, figure 3 shows that a strong peak at 437 obtained between the ranges 400-500 nm for all the SnO_2 samples, which is clear that related to the oxygen vacancy in the spectra. In addition, two weak peaks are observed at 510 and 560nm. The PL studies of SnO_2 nanostructure have been already reported the peaks at 392, 439 and 399nm [11, 12]. Clearly, the present PL spectra showed that have received some difference peaks from previous reports. The emissions at these peaks are obviously not the band-to-band transition because of the wide band gap of bulk SnO_2. The outer electronic structure of Sn is $4d^{10}5s^25p^2$. Hence, the ability of the oxygen atom to combine with Sn atom is nearly the same for approximate outer electronic structure. The uninterrupted contention of the oxygen atom easily leads to the formation of oxygen vacancies and electronic defaults on the interface. Based on the above discussion, the oxygen vacancies really play an important role on PL emission via a recombination of Vo+ electrons with photoexcited holes in the valence band.

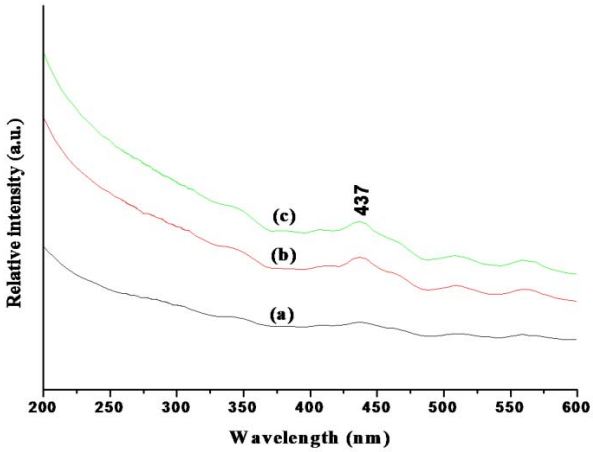

Fig. 3. Photoluminescence spectra of the SnO_2 nanoparticles at different temperatures, (a) 120°C, (b) 200°C and (c) 250°C.

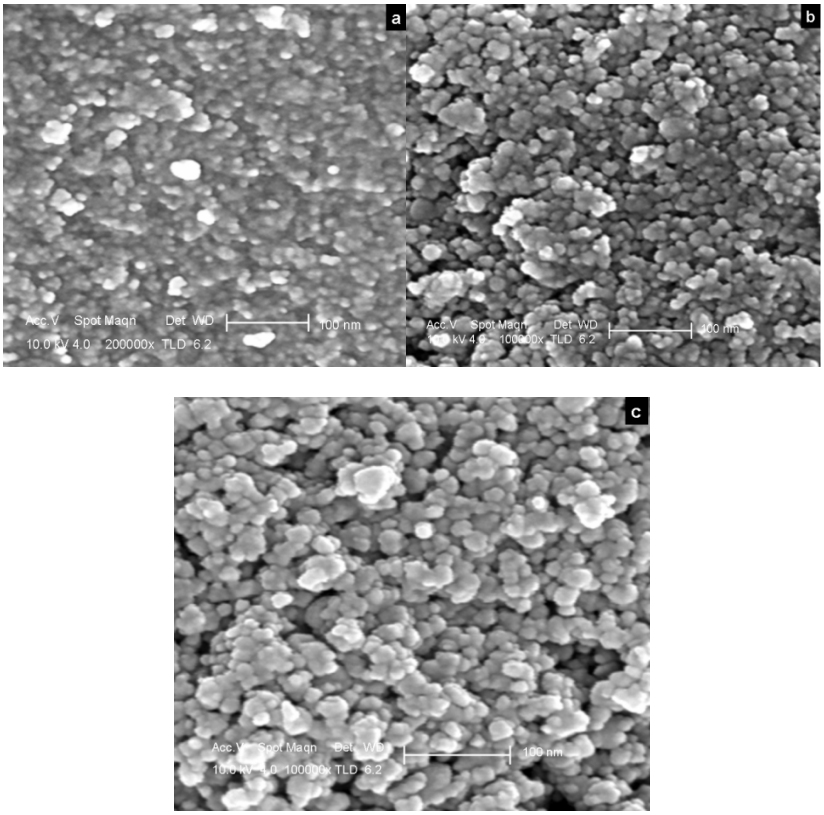

Fig. 4. SEM morphology of the SnO_2 nanoparticles at three different temperatures, (a) 120°C, (b) 200°C and (c) 250°C.

The spherical morphologies were carried out by SEM analysis. Fig. 4 shows the morphologies of samples (a), (b) and (c) with aggregated status. Spherical morphology with a highly porous, foam-like structure can be observed. Particle size of the nanoparticles was drastically decreased from 4.9 sample (c) to 2.4nm sample (a) by the decreasing the preparation temperature.

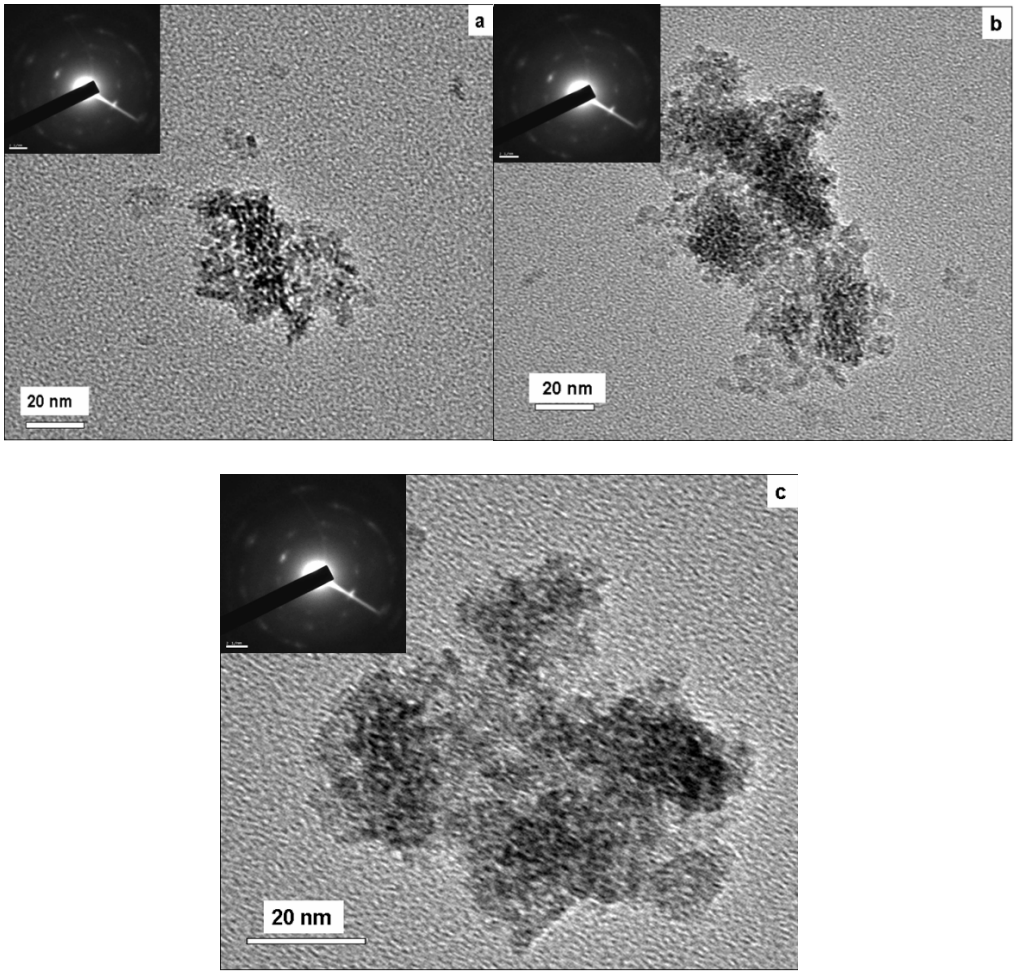

Fig. 5. TEM images of SnO_2 nanoparticles prepared at different temperatures, (a) 120°C, (b) 200°C and (c) 250°C (SEAD pattern inserted).

Fig. 5 (a), (b) and (c) shows the TEM image of as-synthesized SnO_2 nanoparticles by different temperature and corresponding SAED patterns inserted left top corner of the figure. It could be observed from the figure that the nanocrystallite showed extra fine an agglomerated status with mesoporous structures. The size of the primary particles estimated from the TEM images was about 2.4, 4.5 and 4.9nm respectively. Figure 6 (a), (b) and (c) shows HR-TEM of the samples and clear lattice fringes, indicating the established crystallinity of SnO_2 nanoparticles. The distance between lattice fringes were found to be 0.35, 0.26, 0.25nm corresponding to the samples (a), (b) and (c) which was in good agreement with the lattice spacing of (110) plane in the SnO_2 (inset of Fig. 6 (a), (b) and (c)). This is perfectly in agreement with the XRD analytical results, and indicates that the SnO_2 nanoparticles with small average particle sizes were well crystallized. This pattern identifies the poly crystalline nature for the SnO_2 nanocrystals.

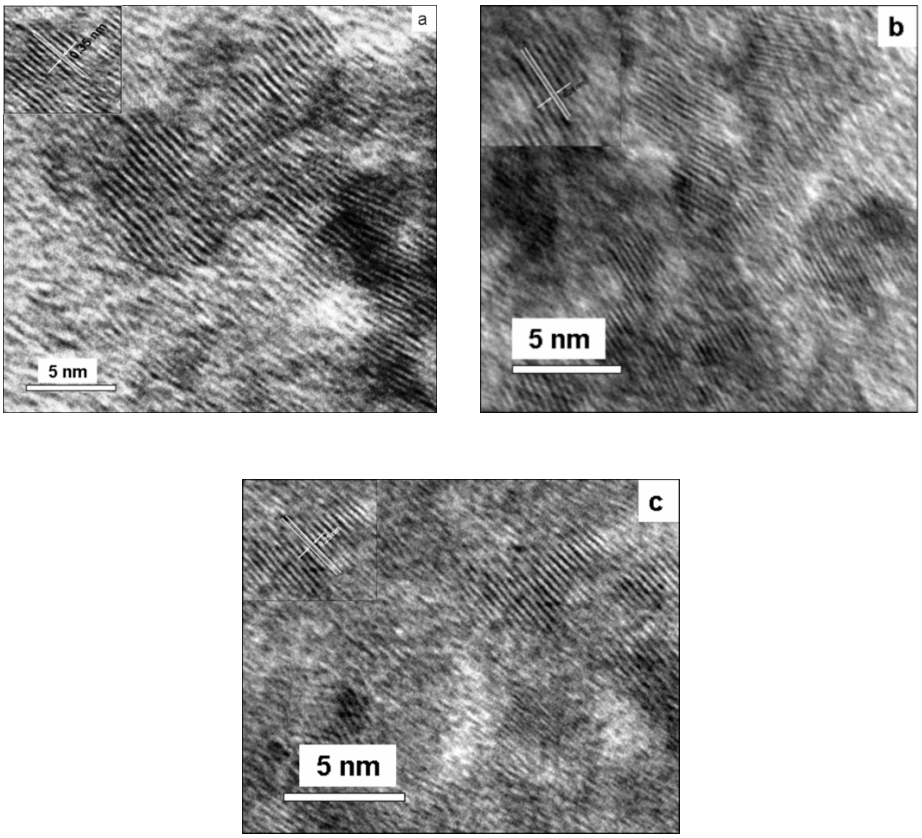

Fig. 6. HR-TEM images of the SnO_2 nanoparticles obtained at different temperatures, (a) 120°C, (b) 200°C and (c) 250°C. The distance between lattice fringes were calculated (inserted).

The formation of nanoparticles can be attributed to the following mechanism. For the tetragonal phase of SnO_2, several groups have indicated that the (110) and (001) surfaces have the lowest and the highest surface energies, respectively [10]. It means that SnO_2 prefer to grow along the [110] direction, forming the SnO_2 nanostructure. In aqueous solution, the concentration of the precursor is extremely low in order to obtain nanostructure. The intermediate products are stabled by alcoholic molecules in the solvothermal method, thus high-yield SnO_2 nanoparticles can be obtained in high concentration precursor. Furthermore, compared with the hydrothermal method, the solvothermal approach using ethanol as the reaction media allows a slower nucleation and growth at lower interfacial tension conditions. Therefore, the solvothermal approach is more favorable to grow c axis elongated anisotropic SnO_2 nanoparticles with high crystal quality [13].

4. Conclusions

In conclusion, tetragonal shape SnO_2 nanoparticles have been successfully prepared by a simple solvothermal method with different temperature condition. Crystallites sizes increased in relation to annealing temperature 2.4, 4.5, and 4.9nm for 150, 200 and 250 °C, respectively. Moreover, average size is slightly small. These sizes, estimated by XRD, are confirmed by the TEM. The morphologies and optical properties of as-synthesized samples have also been investigated by SEM, UV-Vis and PL studies. The temperature can affect the particle size; the decreasing trends of temperature upon the decreasing particle size are well presented for the as-synthesized samples. Moreover, our process directly leads to aqueous suspensions of tin oxide nanoparticles. These suspensions could be used for coating or casting. However, the agglomerate

capability should be evaluated soon. The present method is simple, mild and cheap, which may be suitable for industrial production of high-grade SnO_2 nanoparticles.

Acknowledgement

The authors are grateful to the University of Grant Commission for extending financial assistance to carry out this work.

Reference

[1] Z. Ying, Q. Wan, Z. T. Song, S. L Feng, Nanotechnology **15**, 1682 (2004).
[2] K. L. Chopra, S. Major, D.K Pandya, Thin Solid Films **102**, 1 (1983).
[3] Z. Peng, Z. Shi, M. Liu, Chem. Commun. 2125 (2000)
[4] A. Aoki, H. Sasakura, Japan. J. Appl. Phys **9**, 582 (1970).
[5] B. Cheng, J.M. Russell, W. Shi, L. Zhang, E.T. Samulski, J. Am. Chem. Soc. **126**, 5972 (2004).
[6] A. Gamard, O. Babot, B. Jousseaume, M.C. Rascle, T. Toupance, G. Campet, Chem. Mater. **12**, 3419 (2000).
[7] Z. Chen, J.K.L. Lai, C.H. Shek, H. Chen, Mater. Res. 18, 1289 (2003).
[8] T. Niitz, M. Haase J. Phys. Chem. B 104, 8430 (2000).
[9] K. Vanheusden, W.L. Warren, C.H. Seager, D.R. Tallant, J.A. Voigt, B.E. Gnade, J. Appl. Phys. **79**, 7983 (1996).
[10] F. Gu, S.F. Wang, C.F. Song, M.K. Lu, Y.X. Qi, G.J. Zhou, D. Xu, D.R. Yuan, Chem. Phys. Lett. **372**, 451 (2003).
[11] J.Q. Hu, X.L. Ma, N.G. Shang, Z.Y. Xie, N.B. Wang, C.S. Lee, S.T. Lee J. Phys. Chem. B **106**, 3823 (2002).
[12] J.X. Wang, H.Y. Chen, Y. Gao, D.F. Liu, L. Song, Z.X. Zhang, X.W. Zhao, X.Y. Dou, S.D. Luo, W.Y. Zhou, G. Wang, S.S. Xie J. Cryst. Growth **284**, 73 (2005).
[13] L. Xia, B. Yang, Z. Fu, Y. Yang, H. Yan, Y. Xu, S. Fu, G. Li Mater. Lett. **61**, 1214 (2007).

*Corresponding author: anandphy@yahoo.in